Electrochemical and Solid-State Letters, **10** (11) B196-B200 (2007)
1099-0062/2007/10(11)/B196/5/$20.00 © The Electrochemical Society

An Electro-osmotic Fuel Pump for Direct Methanol Fuel Cells

C. R. Buie, D. Kim, S. Litster, and J. G. Santiago[z]

Department of Mechanical Engineering, Stanford University, Stanford, California 94305, USA

This work reports on the design and performance evaluation of a miniature direct methanol fuel cell (DMFC) integrated with an electro-osmotic (EO) pump for methanol delivery. Electro-osmotic pumps require minimal parasitic power while boasting no moving parts and simple fuel cell integration. Here, an electro-osmotic pump is realized from a commercially available porous glass frit. We characterize a custom-fabricated DMFC with a free convection cathode and coupled to an external electro-osmotic pump operated at applied potentials of 4.0, 7.0, and 10 V. Maximum gross power density of our free convection DMFC (operated at 50°C) is 55 mW/cm^2 using 4.0 mol/L concentration methanol solution supplied by the EO pump. Experimental results show that electro-osmotic pumps can deliver 2.0, 4.0, and 8.0 mol/L methanol/water mixtures to DMFCs while utilizing ~5.0% of the fuel cell power. Furthermore, we discuss pertinent design considerations when using electro-osmotic pumps with DMFCs and areas of future study.
 [DOI: 10.1149/1.2772083]

Manuscript submitted May 24, 2007; revised manuscript received July 13, 2007. Available electronically August 28, 2007.

Direct methanol fuel cells (DMFCs) are attractive energy conversion devices due to the high volumetric energy density of methanol. Benefits for portable applications include long run times, capability for refueling as opposed to recharging, and silent operation.[1-3] Challenges to widespread commercialization include system cost (e.g., pumps, thermal management devices, and packaging), CO_2 removal at the anode, and system efficiency. One approach to reducing cost and improving mechanical reliability is employing passive reactant delivery methods.[4-8] However, for passive systems gaseous CO_2 trapped at the DMFC anode can reduce active catalyst area and lower system power output.[9,10] Also, passive systems are not typically orientation-independent; which is important for portable devices.[11] There is limited published work on active methods of methanol pumping,[12-14] but methanol delivery is a critical area of research and development for portable fuel cells.

We propose the integration of electo-osmotic (EO) pumps with DMFCs. Electro-osmotic flow is the bulk motion of an electrolyte caused by Coulombic interaction of external electric fields and the charges of an electric double layer (EDL).[15] Porous glass EO pumps offer large surface-to-volume ratio and relatively high zeta potential, ζ, defined as the potential drop across the diffuse charges of the EDL. EO pumps have no moving parts and can produce high flow rate per package volume. These properties make EO pumps highly suitable for fuel cell applications. Theoretical and experimental studies on EO pump operation have been presented.[16,17] We recently demonstrated that EO pumps can facilitate water management in H_2/air proton exchange membrane fuel cells.[18,19] Methanol-based solutions have been used in capillary electrophoresis,[20-22] packed-bed EO pumps for liquid chromatography,[23] and monolithic silica EO pumps for electrosprays, and flow injection analyses applications.[24,25] Kim et al.[26] recently studied EO pumping of methanol, deionized water, and other low-conductivity electrolytes. The latter work shows that EO pumps are capable of pumping even pure methanol solutions with relatively high flow rate per power ratios. Recently we presented the first demonstration of an electro-osmotic fuel pump for a DMFC,[27] with a device that featured a pump fabricated from silicon which also served as methanol flow channels. The EO pump in that study supplied adequate methanol but consumed more than the output power of the DMFC. We here describe a new, air-breathing DMFC system with a stand-alone porous glass EO pump.[28]

Experimental

DMFC and EO pump experimental setup.— Figure 1 is a schematic of our DMFC experimental setup. The setup includes an electronic load (Keithley 2410 Sourcemeter), a custom temperature control unit, and a power supply (Agilent 6030A) to control the electro-osmotic pump. The electronic load operates in four-wire sense mode with the source and sense wires connected to the DMFC anode and cathode. The Keithley Sourcemeter is controlled via general purpose interface bus (GPIB) and integrated with LabView 7 using a National Instruments PCI-GPIB card.

In addition to combined DMFC/EO pump experiments, we performed an experimental validation of the EO pump itself to characterize its performance in the regimes of interest. The EO pumps used here are realized from porous borosilicate glass frits (Robu Glasfilter, Germany). The EO pumps are 2.5 cm in diameter, 1.0 mm thick, and have roughly 1.1 μm diameter pores. In these experiments a specified voltage was applied across the EO pump, and instantaneous flow rate was recorded by a Sensirion (Westlake Village, CA) liquid flow sensor. Applied voltage varied from 4.0 to 10 V for 2.0, 4.0, and 8.0 mol/L methanol concentrations (8.1%, 16%, and 32% methanol by volume, respectively). A typical experimental realization consisted of varying the applied voltage from 4.0 to 10 V in 1.0 V increments while allowing the EO pump to operate for 2.0 min at each specified potential. The time-averaged EO pump flow rate and current were obtained during the 2.0 min of operation at each applied voltage. We obtained four realizations per operating condition.

DMFC design.— Figure 2 shows an assembly drawing and a digital image of the components of our air-breathing 2.0 cm^2 DMFC. The cathode current collector is a wire-electrical-discharge-machined (EDM-Tek, Union City, CA), stainless steel 1.0 mm thick plate. The plate has an evaporated gold layer roughly 1.0 μm thick to reduce contact resistance and corrosion. A porous platinum mesh

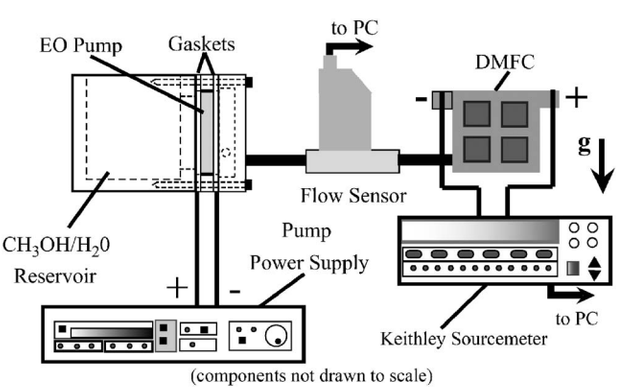

Figure 1. Schematic of the free convection DMFC with EO pump experimental setup including vertically oriented, free-convection DMFC; flow sensor; integrated EO pump and fuel reservoir; pump power supply; and Keithley Sourcemeter (providing fixed current density loads).

[z] E-mail: juan.santiago@stanford.edu

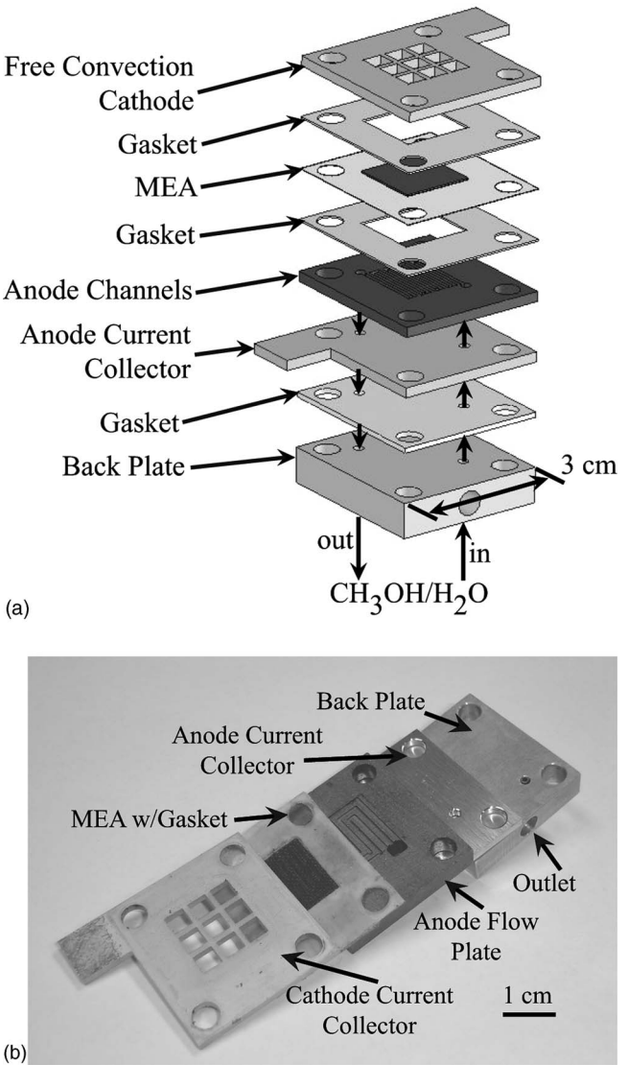

Figure 2. Assembly drawing (a) and digital image (b) of the air-breathing DMFC used in this study. As shown in (a), fuel flows from the EO pump, through the back plate and anode current collector, and reacts at the MEA. The pressure difference generated by the EO pump drives fuel, CO_2, and water through the system and out of the outlet.

(Goodfellow Cambridge Limited, Cambridge, U.K.) was layered on the cathode to reduce ohmic losses due to lateral electron conduction in the gas diffusion layer (GDL).

The membrane electrode assembly (MEA) (BCS Fuel Cells, Inc., Bryan, TX) consisted of a 180 μm thick Nafion membrane (Nafion 117) with 350 μm thick carbon cloth GDLs. The Pt/Ru anode catalyst and Pt cathode catalyst loadings were 4.0 and 2.0 mg/cm^2, respectively. Pt/Ru catalyst was used to improve the relatively slow reaction kinetics of methanol oxidation at the anode. The anode flow field was a graphite plate with end-milled 750 μm wide by 500 μm deep flow channels. The anode current collector was gold-plated copper machined inhouse to fit the structure. The temperature of the cell was regulated at the anode back plate, which included an embedded type K thermocouple and resistive heating element.

Several options are available in the design of fuel cell flow fields and each places unique demands on pumping media. These include (but are not limited to) parallel channels, serpentine channels, combination parallel/serpentine channels, and interdigitated flow fields.[29] Frictional losses translate into higher pressure loads and subsequently, higher EO pump power. We evaluated three anode

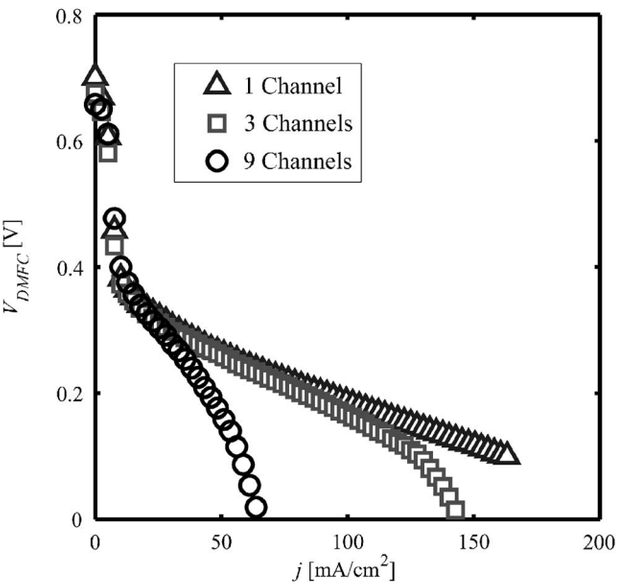

Figure 3. Polarization curves for 2.0 cm^2 DMFCs with nine-, three-, and single-channel anodes. The DMFC operates at room temperature with a 60 μL/min 4.0 mol/L methanol flow rate supplied by syringe pump in each case. Maximum power densities of the nine-, three-, and single-channel designs are respectively 9.2, 17, and 19 mW/cm^2.

flow field designs with parallel (nine-channel), parallel/serpentine (three-channel), and serpentine channels (one-channel). Figure 3 shows room-temperature polarization data for the three flow channel designs fed 4.0 mol/L methanol at 60 μL/min using a syringe pump. For this 2.0 cm^2 DMFC, 60 μL/min corresponds to an anode stoichiometric flow ratio of roughly 12 at 100 mA/cm^2. As shown, the one-channel design displays the highest DMFC potential for a given current. The maximum power of the one-channel design is 10% higher (19 vs 17 mW/cm^2) than the three-channel design. The higher power density of the one-channel design is due to its higher methanol velocity, resulting in improved CO_2 removal at the anode.[30] Given the pressure capability of our pump,[28] we chose the one-channel design, and all of the data below is for this one-channel design.

Results

Electro-osmotic pump evaluation.— Figure 4 shows measurements summarizing the electro-osmotic pump characterization. Here, we operate the EO pump in the absence of the DMFC (i.e., no pressure load). Figure 4a shows maximum pump flow rate as a function of applied voltage for 2.0, 4.0, and 8.0 mol/L methanol solutions. Equations 1 and 2 give the relationship between maximum EO pump flow rate and applied voltage

$$Q_{\max} = -\frac{\psi}{\tau}\frac{\varepsilon\zeta A_{\mathrm{EO}} V_{\mathrm{eff}}}{\mu L} f \qquad [1]$$

$$V_{\mathrm{eff}} = V_{\mathrm{app}} - V_{\mathrm{dec}} - 2R_{\mathrm{A}} I_{\mathrm{EO}} \qquad [2]$$

In Eq. 1, ψ and τ are EO pump porosity and tortuosity, respectively, ε is permittivity of the working fluid, ζ is zeta potential, A_{EO} is the EO pump area, V_{eff} is the effective potential across the pumping substrate, μ is viscosity of the working fluid, and L is pump thickness. The factor f is a nondimensional parameter determined from solutions to the nonlinear Poisson Boltzmann equation describing the EDLs. In Eq. 2, V_{app} is applied voltage, V_{dec} is decomposition potential (the minimum voltage to initiate electrolysis), R_{A} is resistance of the working fluid between the pump and electrode, and I_{EO} is the EO pump current.

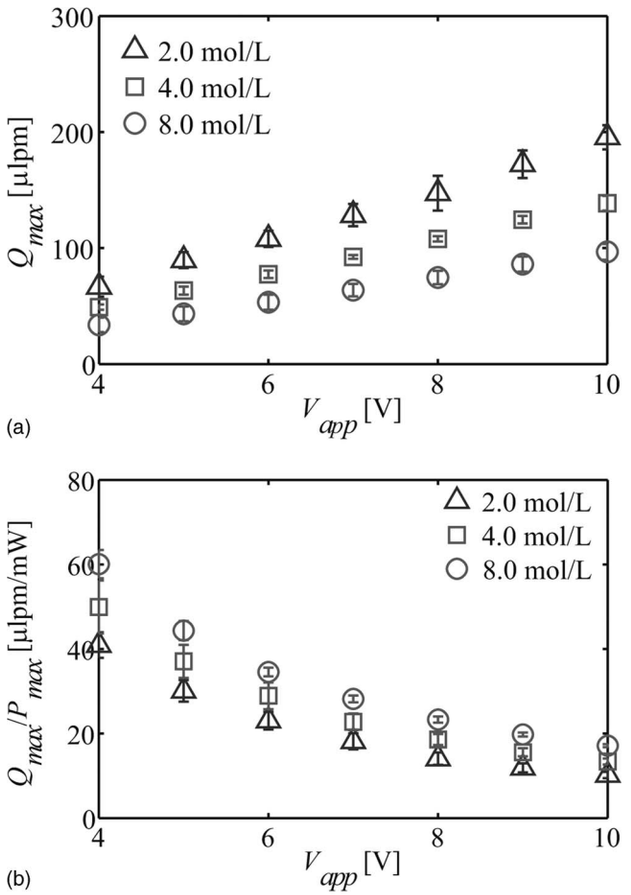

Figure 4. EO pump flow rate (a) and flow rate per power (b) vs applied voltage. As expected, maximum flow rate is a linear function of applied voltage (a), while flow rate per power is approximately inversely proportional to applied voltage (b). The 2.0 mol/L methanol solution yields the highest flow rate at any given voltage (due to its higher ion density and subsequently thinner EDLs), while the 8.0 mol/L methanol case exhibits the highest flow rate per power (due to its lower ionic conductivity). These data highlight the balance between reducing methanol concentration to increase flow rate, and increasing methanol concentration to reduce EO pump power consumption.

Figure 4 shows how the maximum pump flow rate varies linearly with V_{app} for each methanol concentration, as expected. For each applied potential the maximum flow rate decreases with increasing methanol concentration. This trend is consistent with finite EDL effects in relatively small pores with low-ion-density solutions. The parameter f in Eq. 1 varies between zero and unity for increased ion density (f is fixed for a given pumping substrate and working fluid).[16,26] Ion density decreases with increased methanol concentration, as supported by our measurements of conductivity for 2.0, 4.0, and 8.0 mol/L methanol solutions, which yielded values of 2.9, 2.4, and 1.0 $\mu S/cm^2$, respectively. Because ζ is only a weak function of increased methanol concentration,[a] Eq. 1 shows how flow rate decreases with decreasing ion density (decreasing the value of f for finite EDLs).[26]

Figure 4b shows measurements of the EO pump maximum flow rate (Q_{max}) divided by the pump power (P_{max}) consumption for each of the cases shown in Fig. 4a. Equation 3 gives the theoretical formulation of Q_{max}/P_{max}

$$\frac{Q_{max}}{P_{max}} = -\frac{\varepsilon\zeta g}{V_{app}\mu\sigma_\infty} \quad [3]$$

where g is the dimensionless flow rate per current ratio[16,26] and σ_∞ is solution conductivity. Equation 3 predicts an inverse relationship between Q_{max}/P_{max} and V_{app}, which is observed experimentally in Fig. 4b. The value of Q_{max}/P_{max} is highest for the low-conductivity 8.0 mol/L case. We attribute this to the first-order effect of solution conductivity, σ_∞ on Q_{max}/P_{max}, as per Eq. 3.

In Table I we present measurements of maximum EO pump pressure as a function of the methanol concentration and applied potentials studied here. Each maximum pressure measurement is the average of four individual realizations, and the uncertainty limits reflect expected 95% confidence. The expression for maximum EO pump pressure is[16]

$$\Delta p_{max} = -8\varepsilon\zeta V_{eff} f/a^2 \quad [4]$$

Note that maximum pressure is proportional to V_{eff}, unlike maximum flow rate which is proportional to electric field (V_{eff}/L). In general, maximum pressure decreases with increased methanol concentration (due to reduced ion density, thicker EDLs, and subsequently reduced f).[26] Also, for each methanol concentration, maximum pressure increases with applied voltage, as expected from Eq. 2 and 4. Table I also presents estimates of V_{eff} obtained using Eq. 2 and measurements of current and solution conductivity.

Table I. Maximum EO pump pressure measurements.

C_{CH_3OH} (mol/L)	V_{app} (V)	V_{eff} (est.) (V)	Δp_{max} (Pa)
2.0	4.0	0.71	360 ± 26
	7.0	2.8	980 ± 250
	10	4.5	1300 ± 150
4.0	4.0	1.1	390 ± 18
	7.0	3.6	720 ± 26
	10	5.8	1100 ± 120
8.0	4.0	1.2	340 ± 28
	7.0	3.4	640 ± 100
	10	5.4	1100 ± 84

EO pump/DMFC system results.— The EO pump used in our preliminary studies is a commercially available borosilicate glass frit that was not optimized for methanol pumping and yet clearly demonstrates the potential of applying EO pumps to DMFCs. Figure 5 shows typical polarization and power density data for the DMFC supplied with methanol/water solutions by the EO pump. Figures 5a-c show data for the 2.0, 4.0, and 8.0 mol/L methanol concentrations, respectively. We applied EO pump potentials (V_{app}) of 4.0, 7.0, and 10 V to deliver methanol solutions to the DMFC anode. Each polarization curve was obtained in galvanostatic mode with 10 mA steps at 5.0 min per step up to 50 mA; for higher currents, we used 50 mA steps with 10 min per step. (Measurements of polarization curves typically lasted 2.0–2.5 h.) In Fig. 5 the closed symbols (left axis) are the polarization data and the open symbols (right axis) are the gross (not including EO pump losses) output power density data.

Figure 5a shows polarization and gross power density data when the DMFC is fed 2.0 mol/L methanol. At the applied EO pump potential of 4.0 V, the DMFC is starved at the anode (due to the low EO pump flow rate) and the fuel cell voltage falls below 0.30 V before reaching 0.10 A/cm^2. When V_{app} is increased to 7.0 V the

[a] In a future paper we will present zeta potential measurements as a function of aqueous methanol solution concentration for a similar borosilicate glass surface. Between 2 and 8 mol/L methanol concentrations, we estimate zeta potential changes by less than 10%.

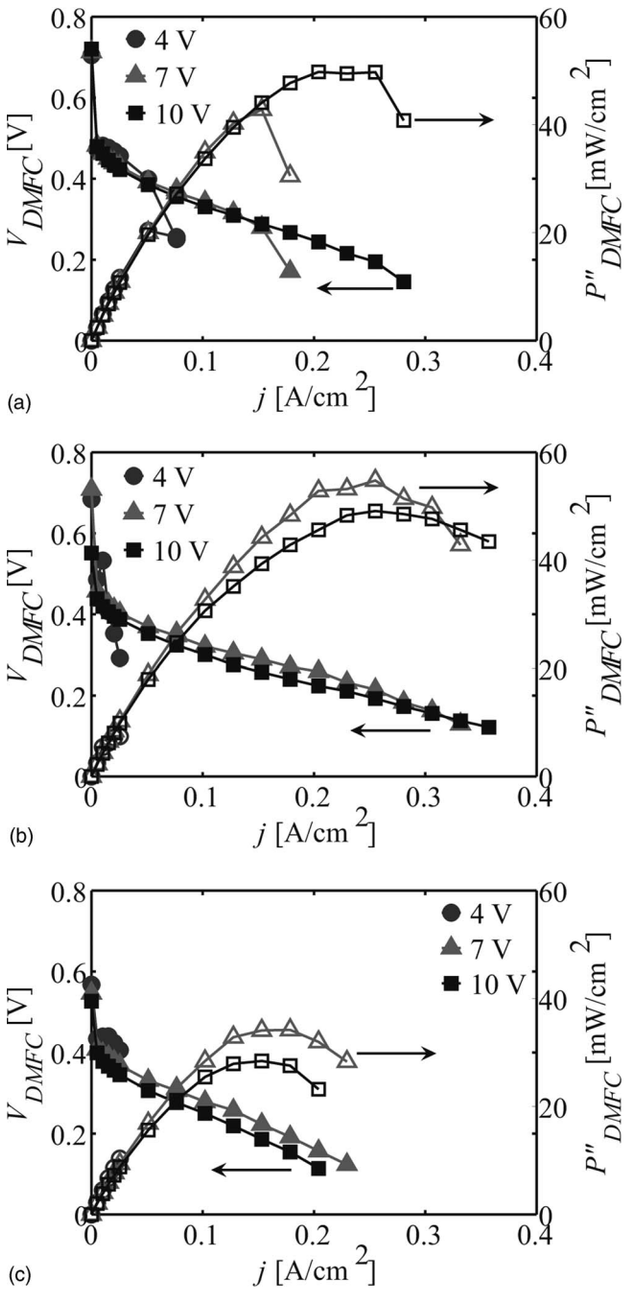

Figure 5. Polarization (closed symbols, left axis) and power density (open symbols, right axis) curves for (a) 2.0, (b) 4.0, and (c) 8.0 mol/L aqueous methanol concentrations. EO pump applied voltages are (○, ●) 4.0 V, (△, ▲) 7.0 V, and (□, ■) 10 V. For each concentration the fuel cell power output was lowest at 4.0 V due to the low flow rate of fuel to the DMFC. For the 2.0 mol/L methanol concentration (a), the DMFC operating range and power density increase with higher V_{app} (corresponding to higher flow rate), with V_{app} = 10 V yielding the highest gross power density (50 mW/cm^2). The maximum gross power density for 4.0 mol/L (55 mW/cm^2) and 8.0 mol/L (34 mW/cm^2) concentrations occurs at V_{app} = 7.0 V. We hypothesize that the 4.0 and 8.0 mol/L cases have a maximum power at a lower V_{app} due to the effects of methanol crossover (and associated reductions in cell potential).

DMFC operating range is extended to nearly 0.20 A/cm^2. For the 2.0 mol/L case the largest operating range and highest gross power density (50 mW/cm^2) occur at V_{app} = 10 V.

The 4.0 and 8.0 mol/L cases (Fig. 5b and c) behave slightly differently than the 2.0 mol/L case. In the 4.0 and 8.0 mol/L cases the fuel cell is starved of methanol at V_{app} = 4.0 V, but the maximum gross power density occurs at V_{app} = 7.0 V, not 10 V as in the 2.0 mol/L case. At lower V_{app}, pump power [which scales as $V_{app}(V_{app}$-$V_{dec})$][16] is low but the fuel cell is deprived of methanol and produces low gross power. At higher V_{app}, fuel cell gross power generally increases, but pump power then scales as $\sim V_{app}^2$ and eventually limits net system power. Furthermore, methanol crossover is enhanced with higher methanol concentration,[31] suggesting a delicate balance between increasing EO pump flow rate (and V_{app}) for improved anodic mass transfer while limiting streamwise-averaged methanol concentration to minimize fuel crossover.

Table II. Measured power performance of the combined EO pump and DMFC system.

C_{CH_3OH} (mol/L)	V_{app} (V)	P_{EO} (mW)	$P_{FC,max}$ (mW)	$P_{FC,net}$ (mW)	$(P_{EO}/P_{FC,max})^*100\%$ (%)
2.0	4.0	1.6	40	38	4.0
	7.0	7.0	84	77	8.3
	10	11	98	87	11
4.0	4.0	0.80	15	14	5.3
	7.0	5.0	110	100	4.5
	10	14	96	82	15
8.0	4.0	0.50	20	19	2.5
	7.0	3.0	67	64	4.5
	10	8.0	55	47	15

Together Fig. 5a-c show the variations of gross system power as a function of methanol concentration and applied pump power. The highest achieved gross power density of 55 mW/cm^2 occurs at V_{app} = 7.0 V for 4.0 mol/L methanol. The maximum power density for the 8.0 mol/L case is considerably lower, 34 mW/cm^2 at V_{app} = 7.0 V. Increases in methanol concentration allow decreased V_{app} but also result in reduced cell potential and reduced gross DMFC power density due to fuel crossover, as in the 8.0 mol/L case. Crossover rate scales roughly with average methanol concentration and crossover decreases DMFC potential.[31]

A summary of the power performance of the combined DMFC and EO pump system is given in Table II. Peak fuel cell power is achieved at intermediate levels of both methanol concentration and pump voltage. The overall maximum net power output (here $P_{FC,net} = P_{DMFC}$-P_{EO} = 100 mW) corresponds to the 4.0 mol/L case at V_{app} = 7.0 V, with a parasitic power ratio of roughly 4.5%. For our system, V_{app} and methanol concentration govern the maximum achievable net power density. This dependence is a function of the complex coupling between pump and cell operation. For a given V_{app}, pump flow rate is a strong function of the hydraulic load imposed by the cell.[16,17] In turn, the pressure drop in the DMFC anode is a strong function of current density, which rules the production of CO_2 gas and required methanol flow rates. Further, fuel cell gross power is a function of both methanol flow rate and inlet methanol concentration (through mass transfer, consumption rate, and crossover effects). All of this makes net system power a complex function of V_{app}, methanol concentration, and other parameters. For all methanol concentrations explored, maximum net power corresponds to the same V_{app} as the maximum gross DMFC power output; a consequence of the fact that EO pump parasitic power is much less than the DMFC power output. As shown in Table II, deviations from 4.0 mol/L concentration and 7.0 V applied potential result in unfavorably high parasitic power, lower fuel cell power output, or both. The data elucidate the balance between these control parameters.

Conclusion

EO pumps can deliver fuel to DMFCs in a compact structure with no moving parts and low parasitic power consumption. These

pumps have the potential to enhance the design space for portable DMFCs. We have shown EO pump performance across a wide range of operating conditions both with and without a DMFC. The EO pump characterization experiments give valuable insight into pump operation with various methanol solutions (2.0, 4.0, and 8.0 mol/L concentrations). Maximum net power is a function of both applied pump potential and methanol concentration, and the maximum achieved net power occurred at intermediate levels of these parameters. Low V_{app} starves the DMFC of fuel, while high V_{app} results in unfavorably high pump power. Low methanol concentration requires higher pump flow rate for the same stochiometry, while overly high methanol concentration increases crossover rate. There is a delicate balance between optimizing pump flow rate per power while maximizing DMFC power output. For the conditions studied, we found the best overall system performance at 4.0 mol/L methanol and EO pump potential of 7.0 V: 100 mW net power output, 50 mW/cm^2 net power density, and 4.5% EO pump parasitic power (P_{EO}/P_{FC}). Several challenges must be overcome before EO pumps will be commercially viable for DMFCs. These challenges include operating the EO pump using DMFC power (e.g., together with a dc-dc converter and power conditioning), management of product gasses generated by the pump (O_2 at the pump anode and H_2 at the cathode), and identification and mitigation of fuel contaminants for minimal solution conductivity. In spite of these challenges, we believe that EO pumps are a promising fuel delivery alternative. The robust aspects of EO pumping (e.g., response to changes in orientation and applied power), manufacturability, and long-term performance are still open questions and interesting areas for future work. Future studies should also focus on optimization and modeling of the combined EO pump/DMFC system to aid in the design of portable fuel cells.

References

1. G. Q. Lu, C. Y. Wang, T. J. Yen, and X. Zhang, *Electrochim. Acta*, **49**, 821 (2004).
2. G. Q. Lu and C. Y. Wang, *J. Power Sources*, **144**, 141 (2005).
3. C. G. Xie, J. Bostaph, and J. Pavio, *J. Power Sources*, **136**, 55 (2004).
4. Q. Ye and T. S. Zhao, *J. Power Sources*, **147**, 196 (2005).
5. Z. Guo and Y. Cao, *J. Power Sources*, **132**, 86 (2004).
6. T. Shimizu, *J. Power Sources*, **137**, 277 (2004).
7. D. J. Kim, *J. Power Sources*, **130**, 172 (2004).
8. Z. Guo and A. Faghri, *J. Power Sources*, **160**, 1183 (2006).
9. C. W. Wong, T. S. Zhao, Q. Ye, and J. G. Liu, *J. Electrochem. Soc.*, **152**, A1600 (2005).
10. P. Argyropoulos, K. Scott, and W. M. Taama, *Electrochim. Acta*, **44**, 3575 (1999).
11. R. Chen, T. S. Zhao, and J. G. Liu, *J. Power Sources*, **157**, 351 (2006).
12. T. Zhang and Q. M. Wang, *J. Power Sources*, **140**, 72 (2005).
13. T. Zhang and Q.-M. Wang, *J. Power Sources*, **158**, 169 (2006).
14. S.-C. Yao, X. Tang, C.-C. Hsieh, Y. Alyousef, M. Vladimer, G. K. Fedder, and C. H. Amon, *Energy*, **31**, 636 (2006).
15. R. F. Probstein, *Physicochemical Hydrodynamics*, John Wiley & Sons, Hoboken, NJ (2003).
16. S. H. Yao and J. G. Santiago, *J. Colloid Interface Sci.*, **268**, 133 (2003).
17. S. H. Yao, D. E. Hertzog, S. L. Zeng, J. C. Mikkelsen, and J. G. Santiago, *J. Colloid Interface Sci.*, **268**, 143 (2003).
18. S. Litster, C. R. Buie, T. Fabian, J. K. Eaton, and J. G. Santiago, *J. Electrochem. Soc.*, **154**, B1049 (2007).
19. C. R. Buie, J. D. Posner, T. Fabian, S.-W. Cha, D. Kim, F. B. Prinz, J. K. Eaton, and J. G. Santiago, *J. Power Sources*, **161**, 191 (2006).
20. T. Okada, *J. Chromatogr. A*, **695**, 309 (1995).
21. I. E. Valko, H. Siren, and M. L. Riekkola, *J. Microcolumn Sep.*, **11**, 199 (1999).
22. P. A. Babay, R. T. Gettar, M. F. Silva, B. Thiele, and D. A. Batistoni, *J. Chromatogr. A* **1116**, 277 (2006).
23. L. X. Chen, J. P. Ma, and Y. F. Guan, *J. Chromatogr. A* **1028**, 219 (2004).
24. Z. Chen, P. Wang, and H. C. Chang, *Anal. Bioanal. Chem.*, **382**, 817 (2005).
25. P. Wang, Z. Chen, and H. C. Chang, *Electrophoresis*, **27**, 3964 (2006).
26. D. Kim, J. D. Posner, and J. G. Santiago, *Sens. Actuators A*, In press.
27. C. R. Buie, Y. Banin, C. Tang, F. B. Prinz, J. G. Santiago, and B. L. Pruitt, in *19th IEEE International Conference on Micro Electro Mechanical Systems*, IEEE, p. 938 (2006).
28. C. R. Buie, D. Kim, S. Litster, and J. G. Santiago, *ECS Trans.*, **3**(1), 1279 (2006).
29. R. O'Hayre, S. W. Cha, W. Colella, and F. B. Prinz, *Fuel Cell Fundamentals*, John Wiley & Sons, New York (2006).
30. C. W. Wong, T. S. Zhao, Q. Ye, and J. G. Liu, *J. Power Sources*, **155**, 291 (2006).
31. X. Ren, T. E. Springer, and S. Gottesfeld, *J. Electrochem. Soc.*, **147**, 92 (2000).